Material extrusion additive manufacturing of recycled discontinuous carbon fibre reinforced thermoplastic composites with different fibre lengths: Through-process microstructural evolution and mechanical property loss

Additive Manufacturing 78 (2023) 103839

Contents lists available at ScienceDirect

Additive Manufacturing

journal homepage: www.elsevier.com/locate/addma

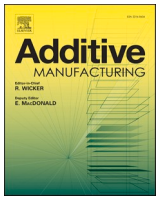

Material extrusion additive manufacturing of recycled discontinuous carbon fibre reinforced thermoplastic composites with different fibre lengths: Through-process microstructural evolution and mechanical property loss

Jiang Wu, Ka Zhang, Dongmin Yang *

School of Engineering, Institute for Materials and Processes, University of Edinburgh, EH9 3FB Edinburgh, UK

ARTICLE INFO

Keywords:
Material extrusion
3D printing
Discontinuous carbon fibres
Recycling
Thermoplastic

ABSTRACT

This paper investigates the evolution of recycled fibres and their influence on the mechanical property loss in material extrusion additive manufacturing of discontinuous carbon fibre reinforced polyamide-6 thermoplastic composites. For the first time, recycled carbon fibres in a broad range of 100 μm - 2.8 mm lengths with a consistent fraction of 20 wt% were produced in composite flakes as feedstock with specific sizes, which were screw-extruded into filament for material extrusion additive manufacturing. Comprehensive characterisations were carried out to trace the evolution of material microstructure throughout the recycling and manufacturing processes. The void content, fibre orientation, fibre length and its breakage were analysed. Tensile tests show that the printed composites with the longest fibre length of 433 μm have the highest tensile strength of 126 MPa and tensile modulus of 6.4 GPa, which are 37% and 63.2% higher than the sample with a conventional 0.1 mm length of milled fibres. Specifically, it was found that the fibre length in 1.4 mm flakes was reduced to 750 μm by screw-extrusion (with customised auger teeth and extruder nozzle) and further reduced to 324 μm by material extrusion (with a nozzle diameter of 1 mm). It has been experimentally identified that the tensile strength of the current 3D printed composites using the initial fibre length of 1.4 mm in coupon can be further increased by more than 55.6% if properly reducing the air voids, fibre breakage and improving the fibre orientation.

1. Introduction

The global recycled carbon fibre market size is predicted to reach USD 222 million by 2026, about 12% growth during the forecast period compared to 126 million in 2021 [1]. Recycled carbon fibres can retain the tensile properties of virgin fibres [2,3], thus they are of high value to be reused in the composites manufacturing industry. At present, recycled carbon fibres produced through mechanical or pyrolysis recycling processes are usually used in the form of discontinuous fibres such as chopped fibres, milled fibres and fibre fragments. Since thermoplastic polymers are possibly 100% recyclable, their combination with recycled carbon fibres can be a sustainable route forward.

Material extrusion (MEX) additive manufacturing (AM) technique, also known as 3D printing, has the potential for the manufacture of recycled fibre reinforced thermoplastic composites, and it offers freedom to fabricate composites with complex shapes [4,5], and fibre distribution and alignment would be improved due to the shearing effects caused by flowing in printing [6], [7–9]. And Fused Filament Fabrication (FFF), as the most cost-effective processes in additive manufacturing, used fabricated filament for the production of functional components. Filament extrusion is utilized in the manufacturing of fibre reinforced composites. However, this process presents challenges as the production of filaments is influenced by process parameters and raw materials. For instance, it has been reported that during filament production, extrusion temperature, nozzle shape, and fibre fraction of the raw materials can impact filament diameter, expansion percentage, and extrusion rate [10]. In previous research, it has been reported that the mechanical properties of virgin discontinuous carbon fibre reinforced composites were affected by fibre types, fibre fraction, matrix type, adhesion between fibres and matrix, distribution of fibres in matrix, hygroscopicity of fibres, fibre aspect ratio, thermal stability, surface energy and thermal expansion coefficient matrix properties [3,11–18] as

* Corresponding author.
E-mail address: Dongmin.Yang@ed.ac.uk (D. Yang).

https://doi.org/10.1016/j.addma.2023.103839
Received 6 April 2023; Received in revised form 16 October 2023; Accepted 18 October 2023
Available online 20 October 2023

well as processing parameters [19,20]. Hence, the production of uniform and stable fibre reinforced filaments is crucial for FFF printing. As for printing, minimising the printing speed, and optimizing nozzle and bed temperature can improve the tensile strength of the printed discontinuous fibre composites [20]. Previous studies have mainly focused on the effects of short fibre fraction and void content on the mechanical properties of short fibre reinforced composites [9,21]. For example, Tekinalp et al. [9] found that the tensile strength and modulus of 3D printed discontinuous CF/ABS composites with a fibre fraction of 30 wt% were improved by 115% and 700%, respectively, as compared to the printed neat ABS polymer. Reclaimed carbon fibre (rCF) reinforced polyamide (PA) composites *via* FFF showed the same trend, with the mechanical properties improved by 243% for tensile strength and 562% for tensile modulus for a fibre fraction of 30 wt% as compared to printed neat PA [6]. Despite that higher fibre fractions are desired in principle for better mechanical performance, existing research has shown that when fibre fraction exceeds 30 wt% more printing defects could be induced in printed composites, resulting in reduced tensile strength [6,9]. This is the case for chopped/milled fibres with a typical average fibre length of around 100 μm, whilst increased fibre lengths may lead to further improved mechanical performance of the printed composites. In discontinuous fibre reinforced polymer composites, the critical fibre length l_c is considered to be the length to obtain the full fibre strength [22], *i.e.*,

$$l_c = \frac{\sigma_{uf} \bullet D}{2\tau} \tag{1}$$

Where $\sigma_{uf}$is the fibre strength, D is the average fibre diameter and τ is the fibre-matrix interfacial shear strength (IFSS). As for carbon fibre and PA6, the critical length is calculated to be 700 μm for a fibre strength of 4000 MPa, a fibre diameter of 7 μm and an IFSS of 20 MPa [23].

However, very few research works were reported to investigate the effect of fibre length on the mechanical properties of FFF printed composites. This was partly because there has been a lack of techniques to produce composite filaments with longer fibre lengths through the existing conventional screw-based extrusion. In addition, due to the variation of extrusion pressure in the printer nozzle, the fibre lengths are difficult to control and maintain during the FFF process. For commercial printer nozzles with standard diameters in the range between 0.4 mm and 1 mm, chopped or milled fibres with a length smaller than the nozzle diameters are used, typically between 100 μm and 200 μm, to avoid potential nozzle clogging [24]. Ning et al. [21] compared the tensile strength of FFF printed composites with two different fibre lengths in a relatively small range (100 μm and 150 μm), and the result showed that the composites with a fibre length of 150 μm provide better tensile properties than 100 μm, with tensile modulus reaching 2.4 GPa and tensile strength of 45 MPa. Krajangsawasdi et al. [25] fabricated highly aligned long discontinuous CF/PLA filament using tapes (with 3 mm constant fibre length) and the tensile strength of printed coupons were reduced by 44.6% (104 MPa) as compared to the filament (188 MPa), which was possibly caused by the additional manufacturing defects induced during the printing, despite, the real fibre length in the printed composites was not characterised and measured.

Due to the limited and scattered results in the literature on FFF printing of discontinuous fibre composites with a broad range of fibre length from microns to millimetres, it is still unclear how the fibre length is reduced during the extrusion and printing processes and how it subsequently affects the mechanical properties of the printed composites. Therefore, this paper aims to experimentally investigate how the fibre length evolves throughout the filament fabrication and the FFF printing processes for composites with an initial fibre length from 100 μm to 2.8 mm. Comprehensive characterisations of the filament and printed composites are carried out to trace the evolution of material microstructures (fibre length, fibre orientation and void content) and establish their relationship with the mechanical property loss of the printed composites through mechanical tests. The paper is organised as follows. Section 2 briefly recovers the theory for predicting fibre efficiency in short fibre reinforced composites. Section 3 presents the experimental methodology including material preparation, filament fabrication, and FFF printing as well as mechanical testing and characterisation. Experimental results for virgin filament and printed composite are presented and discussed alongside the theoretical predictions in Section 4. Conclusions are drawn in Section 5 with suggested future works.

2. Methodology: theoretical

Theoretical predictions from empirical models were used to compare the subsequent experimental results. According to the modified Kelly-Tyson equation, the predicted tensile strength of discontinuous fibre composites with different fibre lengths is calculated by [22]:

$$\sigma_c = \nu_f \cdot \delta_f \left[\left(\sum_{l_i = l\min}^{l_c} \left(\frac{l_i}{2l_c} \right) \right) + \sum_{l_c}^{l_c = l_{\max}} \left(1 - \frac{L_c}{2l_i} \right) \right] + \delta_m (1 - \nu_f) \tag{2}$$

Where σ_c is the tensile strength of composite, δ_f is fibre tensile strength and δ_m is matrix tensile strength, and l_c is the critical fibre length which was mentioned before. ν_f is fibre volume fraction.

It has been understood that the fibre orientation also affects the tensile strength of the discontinuous fibre reinforced composite, which can be considered as an angle ply lamina with off-axis tensile strength being calculated by the modified Tsai-Hill criterion [26]:

$$\sigma(\theta) = \left[\frac{\cos^4\theta}{{\sigma_{11}}^2} + \left(\frac{1}{{\tau_{12}}^2} - \frac{1}{{\sigma_{22}}^2} \right) \sin^2\theta \cos^2\theta + \frac{\sin^4\theta}{{\sigma_{22}}^2} \right]^{-\frac{1}{2}} \tag{3}$$

Where θ is the angle between fibre orientation and loading direction; σ_{11}, σ_{22} and τ_{12} represent longitudinal tensile strength, transverse tensile strength and shear strength of composites, respectively. Under uniaxial tension, σ_{11} becomes σ_c from Eq. (2). And for well-bonded fibres, the composite shear strength was suggested by Purslow [27] that:

$$\tau_{12} = \frac{\tau_m}{(1 + v_f)^2} \tag{4}$$

Where τ_m is matrix shear strength.

The off-axis elastic modulus of composites is determined by:

$$E(\theta) = \left[\frac{\cos^4\theta}{E_{11}} + \frac{\sin^4\theta}{E_{22}} + \frac{1}{4} \left(\frac{1}{G_{12}} - \frac{2\nu_{12}}{E_{11}} \right) \sin^2 2\theta \right]^{-1} \tag{5}$$

Where E_{11} is given below according to the Cox shear-lag model [26]:

$$E_{11} = E_f \left[1 - \frac{\tanh(\beta l/2)}{\beta l/2} \right] v_f + E_m (1 - v_f) \tag{6}$$

Where E_{f} and E_{m} are the elastic modulus of fibre and matrix, and β is given as:

$$\beta = \left[\frac{2\pi G_m}{E_f \left(\pi r_f^2 \right) \ln\left(R/r_f \right)} \right]^{\frac{1}{2}} \tag{7}$$

Where G_{m} is the shear modulus of the matrix, R is the mean separation of fibre length and r_{f} is fibre radius. Where R is the mean inter-fibre spacing.

$$\ln\left(\frac{R}{r_f} \right) = \frac{1}{2} \ln\left(\frac{2\pi}{\sqrt{3}\, V_f} \right) \tag{8}$$

E_{22}, G_{12} and ν_{12} are calculated below.

$$G_{12} = G_m \left(1 + 2\eta_2 v_f \right) / \left(1 - \eta_2 v_f \right) \tag{9}$$

$$E_{22} = E_m(1 + 2\eta_1 v_f)/(1 - \eta_1 v_f) \tag{10}$$

$$\nu_{12} = \nu_f V_f + \nu_m(1 - V_f) \tag{11}$$

Where,

$$\eta_1 = \left(\frac{E_f}{E_m} - 1\right)/\left(\frac{E_f}{E_m} + 2\right) \tag{12}$$

$$\eta_2 = \left(\frac{G_f}{G_m} - 1\right)/\left(\frac{G_f}{G_m} + 1\right) \tag{13}$$

Where ν_f and ν_m is the Poisson's ratio of fibre and matrix, respectively, G_f is fibre shear modulus and $G_m$is matrix shear modulus. Using experimental values measured from Section 2, the theoretical tensile strength σ_c and tensile modulus $E(\theta)$ can be calculated from Eq. (3) and Eq. (5), respectively, which were then used in Section 4 for discussion.

3. Methodology: experimental

3.1. Sample preparation

Screw-based extrusion is a common method to fabricate thermoplastic filaments for FFF printing [28]. In previous research, it has been found that carbon fibre length could be reduced during the mixture and extrusion process [9,29]. In order to ensure a uniform distribution of fibres within the produced filaments, we opted for pre-made composite flakes. This decision was made after considering the challenges associated with directly mixing 3 mm fibre pellets and PA6 pellets. Due to the significant difference in shape between the two types of pellets, the PA pellets tended to prioritize entering the heating barrel, leading to an uneven distribution of fibres. Therefore, the flakes were seized into different sizes such that each type of flake has a specific fibre length. The filament was fabricated using an in-house developed screw-based extruder with a modified nozzle to maintain the fibre length as much as possible and then printed on an FFF printer to produce samples for mechanical tests. A flowchart diagram for the experiment was shown in Fig. 1. More details for each step of the experiment were described below.

3.1.1. Preparation of rCF/PA6 flakes

PA6 pellets (Akulon f136c) were sourced from DSM Ltd. Recycled carbon fibre mats were supplied by Easy Composites Ltd. Before the experiment, PA6 pellets were stored in an oven at 60 ℃ for 12 h to remove moisture. PA6 pellets were spread on the carbon fibre mats in a 300 mm × 300 mm hot press mould. A temperature of 275 °C and a pressure load of 15 kN were used in a hot press (PEI Lab 450) to produce the composite plates. After that, the composite plates were chopped into 10 mm × 10 mm flakes, which were then ground in a grinder at a speed of 27,000 rpm for 6 min. The scraps obtained from the grinder were sieved into different sizes using four meshes in order, *i.e.*, initial fibre lengths of 0.1 mm, 0.7 mm, 1.4 mm and 2.8 mm. This led to four different sizes of recycled carbon fibre reinforced polyamide-6 (rCF/PA6) flakes. In the experiment, 20% weight-fraction flakes were prepared.

3.1.2. Screw-based extrusion of rCF/PA6 filament

Due to the fact that commercially available extruders are often suitable for extruding short fibre reinforced composites, an in-house extrusion system was developed with reference to the RepRapable Recyclebot [30], in order to fabricate discontinuous carbon fibre reinforced polyamide filaments with fibre lengths longer than the 100–150 μm conventional milled fibres. An auger with deep teeth of 5 mm (Fig. 1b) and a DC motor with a torque of 85 Nm were selected for

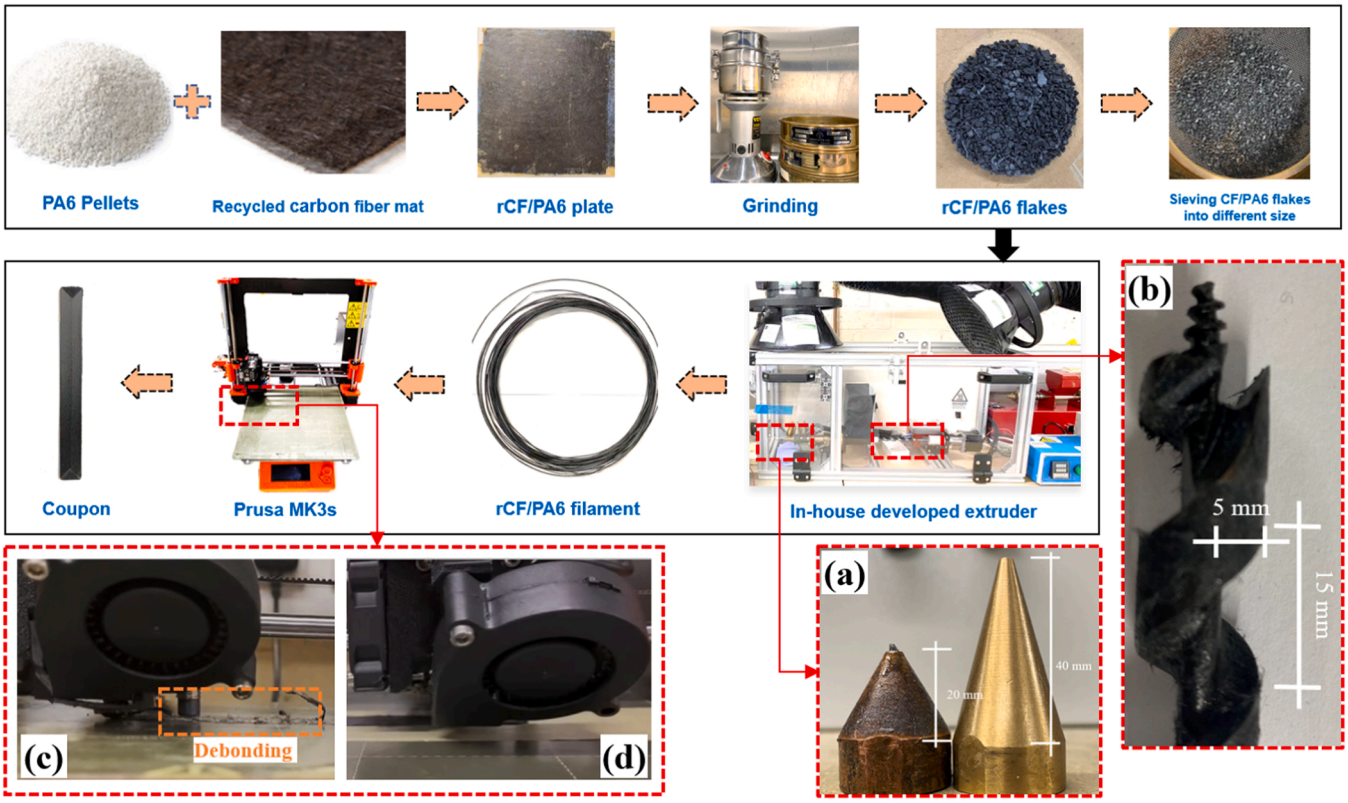

Fig. 1. Flowchart of the experiment from virgin materials, through filament fabrication and printing, to mechanical tests: (a) original extruder nozzle (left) and modified extruder nozzle (right), (b) modified screw auger with deep teeth, (c) raster failed to stick to the bed during printing at 0.4 mm nozzle height, and (d) raster stuck to the bed at 0.3 mm nozzle height.

extrusion to ensure the largest flakes can be pushed into the heating zone. Increasing the depth of the screw is intended to accommodate flakes with the maximum size exceeding 3 mm, ensuring their proper advancement into the heating barrel. And with fibre length increases, the extrusion speed decreases. Therefore, the utilization of a high-power motor is necessary due to the inadequacy of the initially used low-power motor to propel the large-sized flakes into the heating barrel. In addition, the extruder nozzle length was increased to better align the carbon fibres (especially the longer fibres) and avoid the clogging and blockage of long fibres in the nozzle. Specifically, a copper nozzle with a 1.2 mm diameter outlet and 40 mm depth (Fig. 1a) was designed for successfully extruding all the flakes produced above, as a smaller nozzle angle can help to align fibre orientation and reduce the amount of fibre breakage [31], decreasing the cone angle will result in a decrease in axial resistance within the nozzle [32]. The diameter of the extruded filaments was measured to be 1.2 ± 0.4 mm. The selection of filament diameter for filaments is determined by the size of Prusa filament feeding gears.

3.1.3. Material-extrusion based 3D printing

Coupons for tensile tests were manufactured by an FFF 3D printer (Prusa i3 MK3s), as shown in Fig. 1. In order to avoid the blockage and fibre breakage in the printer nozzle when printing longer fibres [24,33,34], a relatively large, 1 mm diameter nozzle was used for all filaments. The nozzle temperature and bed temperature were set as 275 °C and 110 °C, according to the datasheet of Akulon f136c respectively, and the printing speed was set as 15 mm/s since a low deposition speed can help to enhance the adhesion of filament and avoid defects in the printed composite coupons. According to Krajangsawasdi et al. [25] a low nozzle height would cause a matrix-rich area and change the raster width. During the printing experiment, it was found that a lower nozzle height and a higher flow rate tended to cause nozzle clogging as the fibre length and volume fraction increased. In addition, the deviation of the filament diameter would also cause the filament to bend during the filament feeding process, leading to occasionally insufficient feeding forces and thus more likely blockages in the nozzle. After a few trials it was found that at a nozzle height of 0.4 mm, the printed filament (fabricated by flakes with 1.4 mm initial fibre length) failed to stick to the previous layer (see Fig. 1c), whereas a conventional nozzle height of 0.15 mm [21] caused the nozzle clogging issue. As such the nozzle height of 0.3 mm was found suitable for successfully printing out the filaments with a fibre content of 20 wt% (see Fig. 1d). It should be noted that this study aims to explore the effect of fibre length and orientation on the tensile properties of FFF printed composites, therefore it was decided to use consistent printing parameters for printing all samples with the same fibre content. However, 0.3 mm nozzle height was not necessarily optimal for very short fibre reinforced filaments (*e.g.* fibre length less than 200 μm) as it would induce more defects in the printed composites such as air voids and weak bonding between adjacent printing beads [33,34]. Despite this, nozzle clogging still occasionally occurred with the 0.3 mm nozzle height. As we increased the fibre length, existing FFF printing process proved incapable of fabricating the desired composite structures. The polymer and fibres completely blocked the printer nozzle. Therefore, with the current printing set-up (*i.e.*, nozzle diameter around 1 mm and layer height around 0.3 mm), it is not possible to achieve fibre lengths exceeding 0.7 mm through FFF printing. However, it may be feasible to achieve fibre lengths exceeding 0.7 mm by considering lower volume fractions, such as 5%− 7% fibre volume fraction, but this is out of the scope of the current study. The printing path is auto-designed and extrude volume rate is improved to 150% in Cura, to avoid uneven extrusion caused by uneven filament diameter.

3.1.4. Hot-press post-processing

As the theoretical formula only considers fibre orientation and does not account for porosity, the hot-pressed coupons and filaments will be included in the experiments to study the factors contributing to the reduction in mechanical performance of discontinuous fibre reinforced composites during FFF printing. This decision is based on the consideration that the hot-pressing is more mature for manufacturing discontinuous fibre reinforced composites compared to FFF printing. The mechanical properties of the samples obtained through hot pressing, including the coupons and filaments, are expected to be closer to the theoretical values. This is because the hot pressing reduces porosity, which is a factor that can adversely affect the mechanical performance of the composites. Furthermore, the aligned fibre orientation achieved during FFF printing is preserved during the hot pressing, minimizing the deviations from the theoretical predictions. The selected FFF printed samples and filaments were post-processed in moulds with a hot press (PEI Lab 450) machine, with the intention to reduce the porosity and investigate how porosity would contribute to mechanical property loss. The samples were hot pressed with 210 °C and 1 kN press force for 20 min, and the temperature gradient is 10 °C/min. The temperature-pressure processing parameters were adopted from Pascual-González et al., [35] for CF/PA6 composites.

3.2. Mechanical tensile tests

Each coupon has a design size of 150 mm × 16 mm × 1 mm, according to ASTM D3039 [36] (tensile test for polymer matrix composite material reinforced by high-modulus fibres), instead of the ASTM D638 [37] for composites [38]. The mechanical tensile tests were performed at a strain rate of 2 mm/min on an Instron 3369 machine with a 10 kN load cell. For each sample, three coupons were prepared and tested to avoid randomness. All coupons were dried in an oven at 60 °C for 12 h before the test to remove the moisture.

3.3. Characterisation of microstructures

Morphology including fibre length, fibre orientation and void content of 20 wt% samples were characterised and measured to trace their evolution throughout the experimental processes and quantify their influences on the mechanical property loss in FFF printed 20 wt% rCF/PA6 composites.

Composite filaments and printed coupons were soaked with formic acid in bottles. After PA6 was dissolved the formic acid was extracted with a dropper and placed on a glass slide. Once the formic acid evaporated the remaining fibres were observed under an optical microscope (Axioskop 2 Optical, ZEISS) and SEM (TM4000Plus, HITACHI). Fibre lengths need to be manually measured, therefore at least 1000 fibres counted for each sample for statistical purposes [39,40]. Details are shown in Appendix A.

To measure the void contents, after composite filaments were sanded and polished, the cross-section of samples was observed under the microscope (Axioskop 2 Optical, ZEISS). In addition, porosity V_p of coupons was also calculated according to the volumetric porosity equation [6]:

$$V_p = \left(1 - \frac{\rho_m}{\rho_t}\right) \times 100\% \tag{14}$$

Where ρ_m is measured density and ρ_t is theoretical density. Samples were cut into regular shapes. Dimensions were measured to calculate the volume and mass was weighed on a digital balance scale (Adventurer™, Ohaus). Average density was then calculated for all coupons. The recycled carbon fibre and PA6 had a density of 1.36 g/cm^3 and 1.13 g/cm^3, therefore the composite had a corresponding theoretical density of 1.17 g/cm^3 for a fibre content of 20 wt%. The longitudinal section images of samples were observed [41]. Each fibre in the image was identified and its angle with respect to the initial build orientation was measured, where the average angle of all fibres was considered as the initial direction of samples (Appendix A).

4. Results and discussion

4.1. Evolution of fibre length

Fig. 2 illustrated the statistical distributions of fibre length for all filaments and printed coupons. The initial fibre length in the flake was assumed to be close to the size of the seized flakes, and for better clarification, the filaments and printed coupons were labelled according to the size of the flakes, *i.e.*, 1.4 mm filament and 1.4 mm coupon referred to the filament and coupon made from the 1.4 mm size flake. For the first two cases with initial fibre lengths of 0.1 mm and 0.7 mm, it was found that the fibre lengths were much more concentrated between 0.1 mm and 0.2 mm, thus smaller intervals were used for the range below 0.2 mm whilst coarser intervals were used for the range above 0.2 mm. This led to better contrast and comparison of the fibre length distributions (in terms of μm) in the filaments and coupons as shown in Figs. 2a and 2b, with intervals including [0,100], [100,200], [200,700], [700,1400], [1400,2800] and [2800,5000]. When long fibres were used in the cases of 1.4 mm and 2.8 mm, the fibre length distributions were found to flatten out with more concentrations in the range between 0.1 mm and 0.7 mm, thus an insert of 0.3 mm was used instead, which eventually led to the intervals of [0,100], [100,300], [300,700], [700,1400], [1400,2800] and [2800,5000].

In general, longer fibres were more likely to be fragmented during both the screw-extrusion and FFF printing processes [42]. For all four cases with a fibre fraction of 20 wt%, the fibre length was reduced. When very short fibres were used in the case of 0.1 mm initial fibre lengths, the majority of the fibres have a length below 200 μm in both filaments and printed coupons (see Fig. 2a). After printing the fibre length distribution was slightly spread out but still concentrated in the [100,200] domain. A similar trend can be seen for the case of 0.7 mm initial fibre length in Fig. 2b, except more fibres were found to preserve a length between 100 μm and 200 μm after FFF printing, as compared to the case of 0.1 mm.

When relatively longer fibres, such as 2.8 mm long fibres, were used in screw-extrusion (see Fig. 2d), the peak frequency of fibre length was shifted to the domain of [300,700] in the filament, with noticeable distributions in the domains of [700,1400] and [1400,2800]. The distributions showed that the majority of the fibres experienced severe breakage, with only about 21.1% and 3.6% of fibres preserving the initial fibre length of 1.4 mm and 2.8 mm, respectively. The fibre length was further reduced after FFF printing, leading to a more narrowed distribution centred at [100,300] for the 1.4 mm case and [300,700] for the 2.8 mm case. It should be noted that in the case of 2.8 mm initial fibre length, a substantial amount (~39.6%) of fibres preserved a length between 100 μm and 300 μm, and 45.1% fibres have a length between 300 μm and 700 μm. The average fibre lengths for printed coupons were 145 μm, 248 μm, 324 μm and 433 μm, respectively.

Fig. 3 shows the evolution of average fibre length, from flakes through filaments to the final coupon, for the case of 1.4 mm initial fibre length as an example. It can be seen that the average fibre lengths in the flake were very close to the initial length. Although the carbon fibres were hot pressed with PA6 and chopped into flakes with similar sizes before feeding to the screw extruder, the fibre lengths were still reduced during the extrusion processing, resulting in a lower average fibre length in the filament (*i.e.*,750 μm). The average fibre length was further

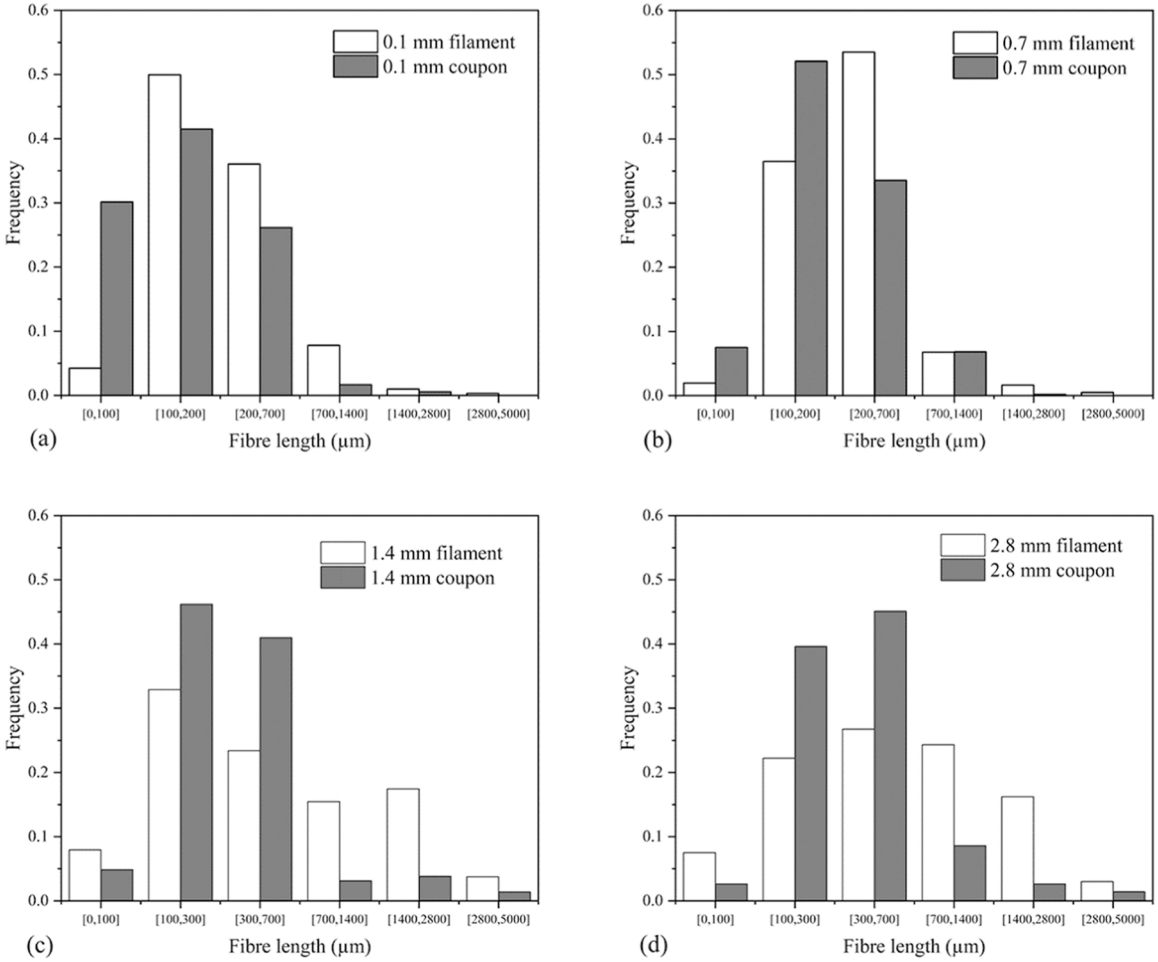

Fig. 2. Evolution of fibre length distribution in filaments and coupons.

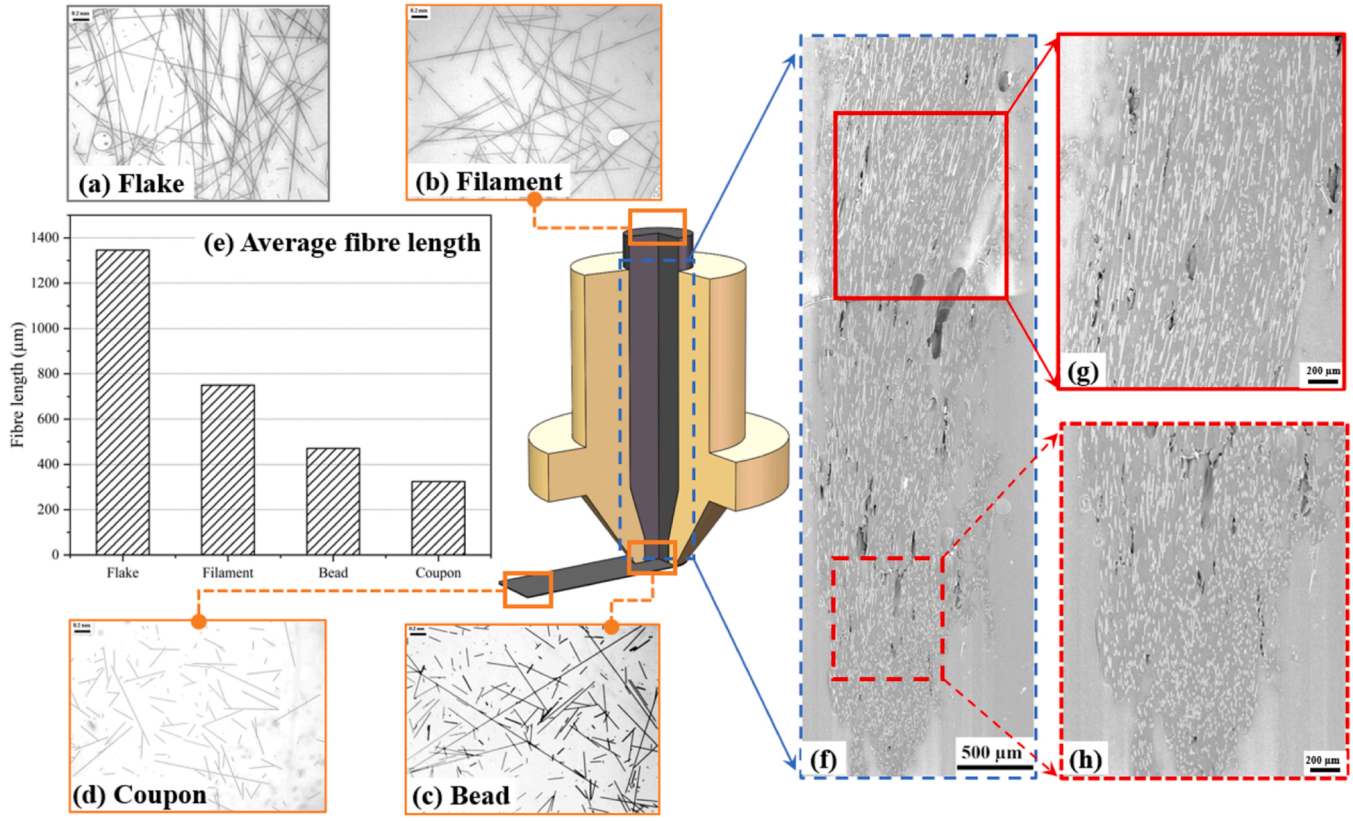

Fig. 3. Microscopic images of fibre length of (a) flakes, (b) filaments and (c) bead and (d) coupons of 1.4 mm initial fibre length samples, (e) evolution of average fibre length in the case with an initial fibre length of 1.4 mm, (f-h) SEM image showing obvious reduction of displayed fibre length in printer nozzle during extrusion processing.

reduced to 324 μm after printing. With the same printing conditions (1 mm nozzle and 0.3 nozzle height), compared to short fibre breakage during FFF processing (81 μm fibre length in filament reduced to 76 μm during FFF) [34], longer fibre breakage appears to more severe (750 μm fibre length in filament reduced to 324 μm during FFF). In order to better identify the reason for fibre breakage in the FFF printing process, the fibre length of the extruded bead above the printer bed was also measured, *i.e.*, 471 μm. This confirmed that fibre breakage occurred in the printer nozzle during extrusion, due to the interaction between fibres as well as the collision between the fibres and the nozzle internal wall surface [9,13,33,43]. Unlike short fibre breakage during the deposition stage [34,38], it was identified (by extracting the filament from the nozzle and examining it by SEM in Fig. 3f) that the long fibres already experienced severe breakage. This indicates that the fibre breakage during the FFF process occurs in two stages. The first stage is caused by the extrusion pressure in the nozzle. After the breakage, if the reduced fibre length after stage 1 is printable with the printing parameters (for example, the reduced fibre lengths after the first stage can be printed successfully with a 1 mm nozzle diameter and 0.3 mm nozzle height in this experiment), the polymer and fibres will enter the second deposition stage and suffer another breakage. The second-stage fracture may be influenced by the ratio of layer height to fibre length in the printing process. In this study, the majority of fibre lengths were significantly greater than the printing layer height. And it is indicated that under the same fibre length, reducing the layer height can result in more severe fibre fracture [34]. This can explain why the nozzle is more prone to clogging at lower nozzle heights, as the fibre length after the first stage of breakage may not satisfy the conditions for lower nozzle heights.

4.2. Morphological analysis

Fig. 4a, b, c and d depict images of the longitudinal section of rCF/PA6 filaments. It is evident that when the fibre length is under 1.4 mm, the filament exhibits better geometric shape and fibre alignment. Specifically, the diameter of filaments with an initial fibre length over 1.4 mm exhibits poorer uniformity, as shown in Fig. 4c and d. For filament with an initial fibre length of 2.8 mm, the diameter substantially varies in a big range between 0.99 mm and 1.3 mm. Furthermore, the fibre alignment in Fig. 4c and d is worse compared to Fig. 4a and b. This finding aligns with the work by Sam-Daliri et al. [44] that the aspect ratio of the fibres can influence the uniformity of filament diameter. The printed coupons exhibit a similar trend in Fig. 4e, f, g and h. In coupons with an initial length of 0.1 and 0.7 mm (Fig. 4e and f), the fibre distribution is uniform. However, as the fibre length increases, the distribution of fibres becomes more uneven, and the alignment becomes more disordered, as shown in Fig. 4g and h. Some of carbon fibres are pull out during polishing process, as shown in Fig. 4h. This may be attributed to poor fibre alignment and weak fibre/matrix interfacial bonding. Additionally, there are more visible voids in coupons with an initial fibre length over 1.4 mm, as shown in Fig. 4g and h compared to coupons with an initial fibre length under 1.4 mm (Fig. 4e and f). This is in agreement with what has been reported by Sam-Daliri et al., [44] that a higher aspect ratio can result in reduced flow rates and increased porosity due to nozzle clogging.

4.3. Evolution of fibre orientation

The fibre orientations are represented as B-spline curves in Fig. 5. It was reported in our previous work that the fibres are generally well aligned in the filament with a fibre length of 118 μm, however, after FFF

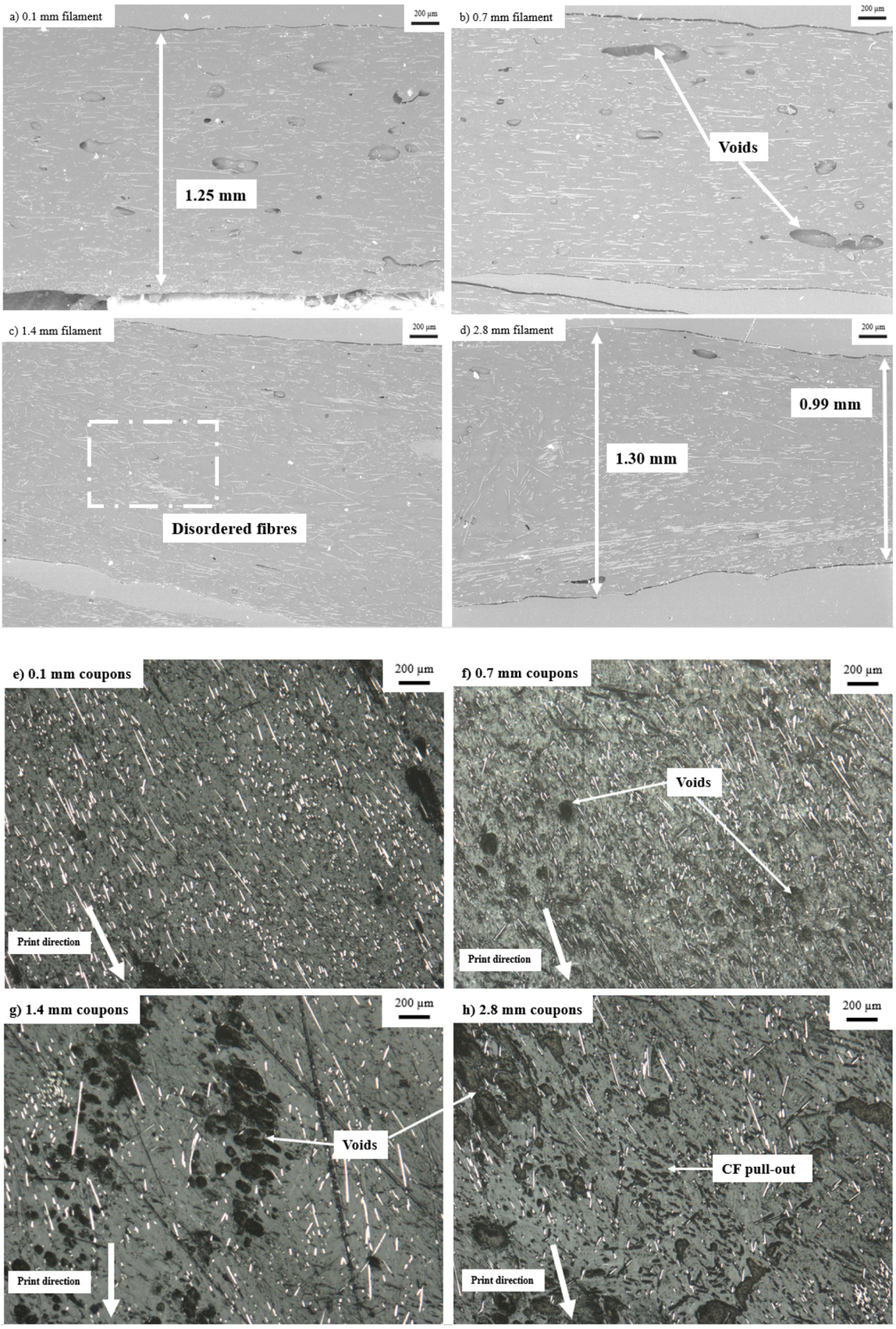

Fig. 4. SEM images of longitudinal section of filaments (a-d) and microscopic images of longitudinal section of coupons (e-h).

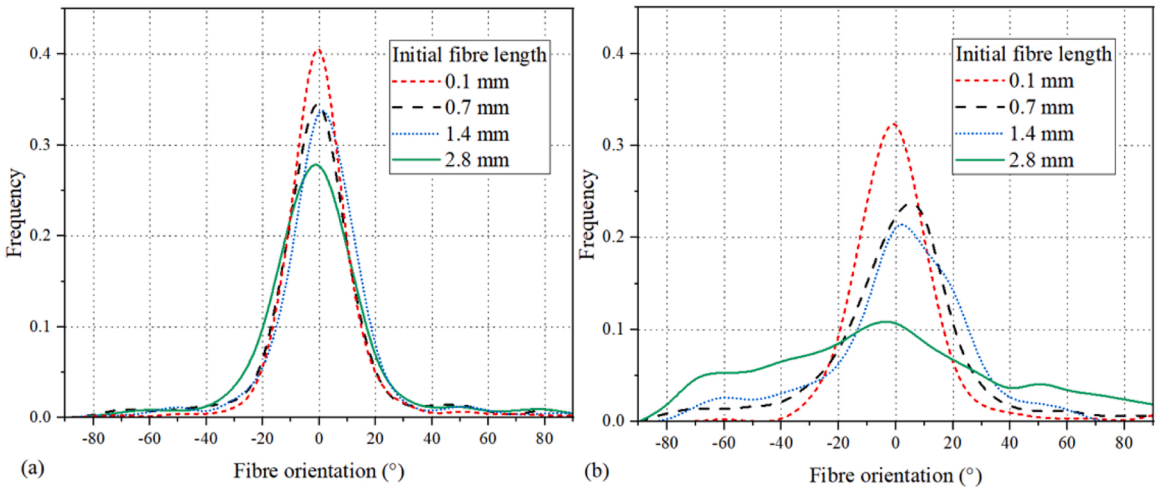

Fig. 5. Evolution of fibre orientation in (a) filaments and (b) coupons.

printing fibre orientation becomes more disordered [33]. Fig. 5 showed the evolution of fibre orientation in filament and coupon with different fibre lengths. It can be clearly observed that the fibre orientation in the filaments (with the same diameter) was slightly decrease with the increasing fibre length, with similar Gaussian distributions as shown in Fig. 5a. This may be attributed to a decrease of the filament uniformity as shown in Fig. 4d. After FFF printing, composite coupons showed much more disordered fibre orientation, especially for the case with an initial fibre length of 2.8 mm, where the printed composite became highly anisotropic (see Fig. 5b).

4.4. Evolution of porosity

Fig. 6 illustrates that the porosity increased with the fibre length and fraction in the filaments. This was due to the fact that carbon fibres increase the viscosity and reduce the flow-ability of the polymer [39, 45], impeding the melt flowing and the degassed air caused the increasing porosity during the extrusion process [39]. It has also been reported that an increase in the length of fibres increases the loss modulus of polymers, indicating that longer fibres result in increased viscosity and slower flow [46]. Similarly, the porosity also increased as fibre length increaseed in the FFF printed coupons. It has been reported that FFF printing could reduce the voids inside the raster and enhance the bonding interface between the fibre and the matrix when printing very short fibres, *e.g.* 118 μm [33]. However, as a constant 1 mm diameter nozzle was used in this study at a relatively high nozzle height of 0.3 mm to allow the printing of longer fibre composites (*e.g.* the case with 2.8 mm initial fibre length), the printing parameters were not intentionally optimised and thus tended to cause more voids between each raster. As a result, there appeared to be very high porosity in the printed composites with initial fibre lengths 1.4 mm (17.77%) and 2.8 mm (17.11%), which consequently would negatively affect their tensile properties. It is worth noting that as the initial length increased from 0.1 mm to 0.7 mm, the porosity showed a reduction for filaments. The process of manufacturing filaments using a screw-based extruder is complex and is influenced by factors such as the temperature distribution within the heating barrel, extrusion speed and other environmental factors. During the experimental process, there may be variations in the actual operating conditions of the extruder, and the distribution of voids within the filaments is more random, leading to disparities between the actual porosity and the expected results. However, when considering the porosity results of both the filaments and the coupons, the porosity values for 0.1 mm and 0.7 mm are close, and they exhibit significant differences compared to the 1.4 mm and 2.8 mm groups. Therefore, this does not affect the conclusion that fibre length influences porosity.

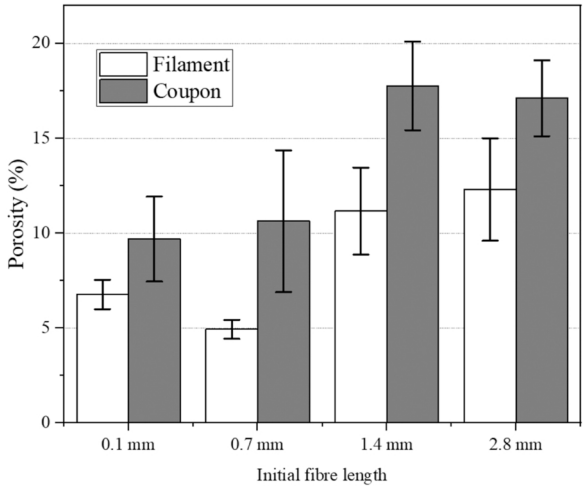

Fig. 6. Evolution of porosity in filaments and coupons.

4.5. Mechanical property loss

The fibre length, fibre fraction, fibre orientation as well as porosity collectively determines the mechanical properties of the FFF printed composites. To theoretically calculate the tensile strength and modulus of the FFF printed composites using different lengths of fibres, the experimentally measured porosity and fibre orientation of the printed composites, which were summarised and plotted in Fig. 7a, and fibre orientation was used in Eq. 3 and Eq. 5, assuming the perfect fibre/matrix interfacial bonding and zero air voids.

The experimentally measured tensile strength and tensile modulus of the FFF printed composites were plotted in Fig. 7b. A representative stress-strain curve for each case was also plotted in Fig. 7c (see the insert), which shows the elongation (failure strain) was reduced with the increased fibre length. As expected, the longer fibres gave rise to both the tensile strength and tensile modulus. The FFF printed composites with very short, 145 μm fibres reached a tensile strength of 92 MPa and tensile modulus of 3.94 GPa. The printed composites with a measured average fibre length of 433 μm (corresponding to the initial fibre length of 2.8 mm) reached the highest tensile strength of 126 MPa and tensile modulus of 6.43 GPa. However, these were still lower than the theoretical values (152 MPa) due to the presence of printing defects, including porosity, anisotropic fibre orientation (as shown in Fig. 7a) and possible weak fibre/matrix interfacial bonding. According to the

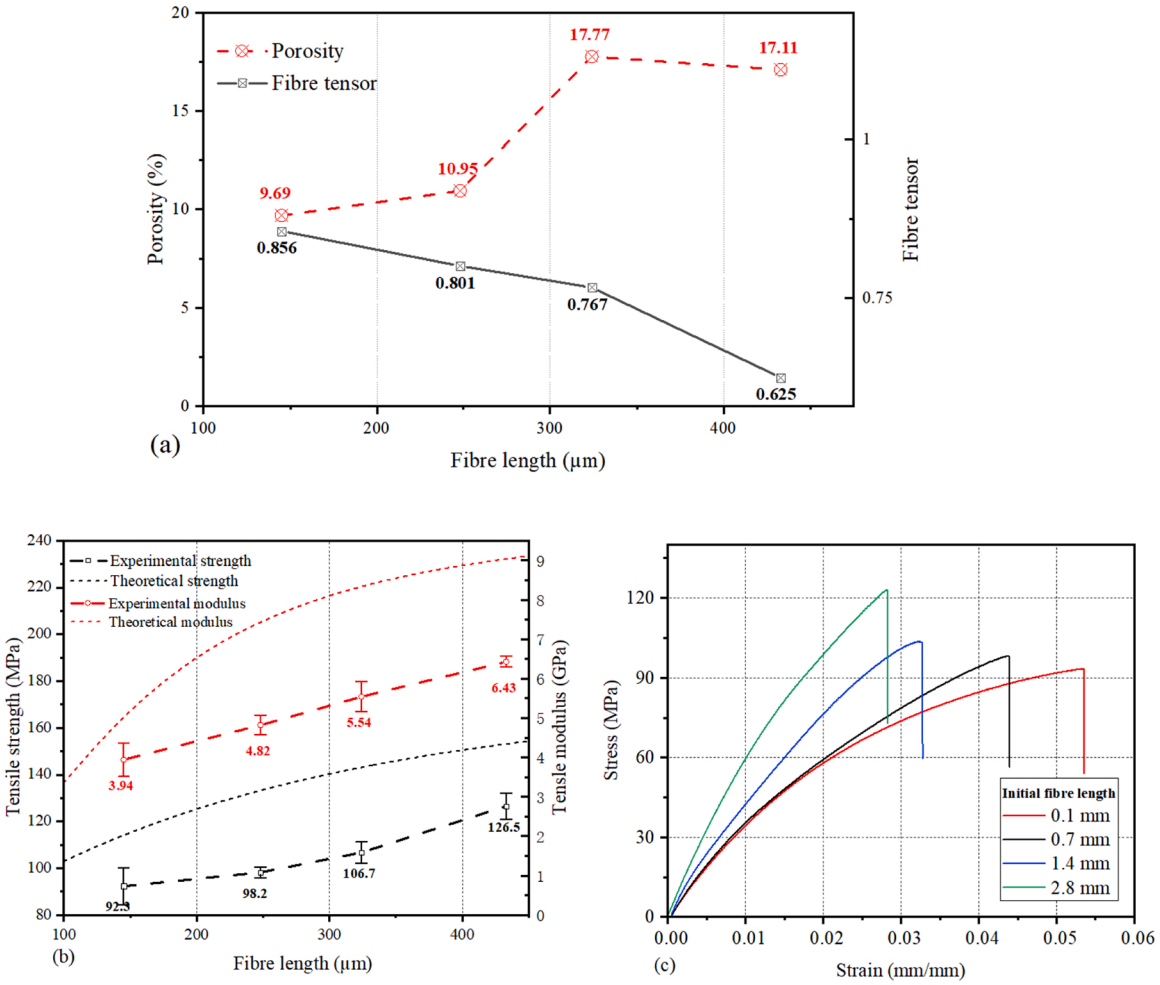

Fig. 7. (a) Experimentally measured average microstructural properties, (b) experimentally measured and theoretically predicted tensile strength and modulus, and (c) stress-strain curve of printed coupons with different (measured) fibre lengths.

modified Tsai-Hill theoretical model, the tensile strength of FFF printed 20 wt% rCF/PA6 composites with an initial fibre length of 2.8 mm still have room of 20.6% for improvement. Generally, the experimental results showed a very similar trend with the theoretical predictions. As the maximum fibre length (433 μm) was still below the critical fibre length, there was not a clear transition point for the tensile properties to converge.

The fracture surface images after the tensile test were shown in Fig. 8. The samples with 1.4 mm and 2.8 mm initial fibre lengths clearly showed much more anisotropic fibre orientation and fibre length than samples with 0.1 mm and 0.7 mm initial fibre lengths. In addition, in the cases of 0.1 mm and 0.7 mm initial fibre lengths, there appeared to be a large amount of fibre pulling-out events. In contrast, there were more unimpregnated carbon fibres in the longer fibre reinforced coupons (Fig. 8c and Fig. 8d). This could be one of the factors causing the tensile properties lower than theoretical predictions. Since no surface treatment was adopted in this study for the recycled carbon fibres in all cases, the fibre/matrix interfacial strength would be weaker than the matrix strength [47]. It has also been reported that the FFF printing process can weaken the fibre/matrix interface [23,48]. Therefore, fibre/matrix debonding and fibre pulling-out would tend to occur rather than fibre breaking, this is caused by the interfacial shear stress at the fibre end [49], noting that the maximum fibre length is smaller than the critical fibre length. Therefore, improving the fibre orientation and fibre/matrix interfacial bonding would reduce the mechanical property loss in FFF printing of rCF/PA6 composites.

FFF printed composites with an initial fibre length of 1.4 mm were hot pressed to remove the printing-induced porosity as much as possible and identify the contribution of porosity to the mechanical property loss. Fig. 9 shows the porosity in the printed composites after hot press treatment was reduced to 8.9%, from an initial value of 17.77% (as seen in Fig. 6). And Fig. 9 shows the tensile strength was substantially improved by 23.6% after hot press because of the porosity reduction. After hot press processing, the tensile strength of coupons got closer to the theoretical strength, confirming that the void content caused the mechanical properties loss as presented in Fig. 9. The mechanical loss for this part can be readily avoided by adjusting the printing parameters, as the porosity level of 8.9% in this condition falls within the acceptable range of porosity for commonly printed discontinuous fibre composites. However, it still existed improvement room compared to the theoretical strength, caused by the existing 8.9% porosity and weak interfacial shear strength.

The virgin filament with an initial fibre length of 1.4 mm was also hot pressed to investigate how much space for improvement in tensile strength in the most ideal state. The tensile strength of the hot-pressed filament was found to be 166 MPa, which is 26% higher than that of the printed composites after hot pressing. As measured before, the average fibre length was reduced from 750 μm in the virgin filament to 324 μm in the printed composites (see Fig. 3) and porosity is reduced to 1.9%. However, addressing the loss in this part may require further improvements in the printing process or change printing technique to avoid. Due to the fibre breakage occurs during two stages, they can be considered separately. In the first stage, fibre breakage occurs due to back pressure exerted on the fibres. This can be achieved by reducing the

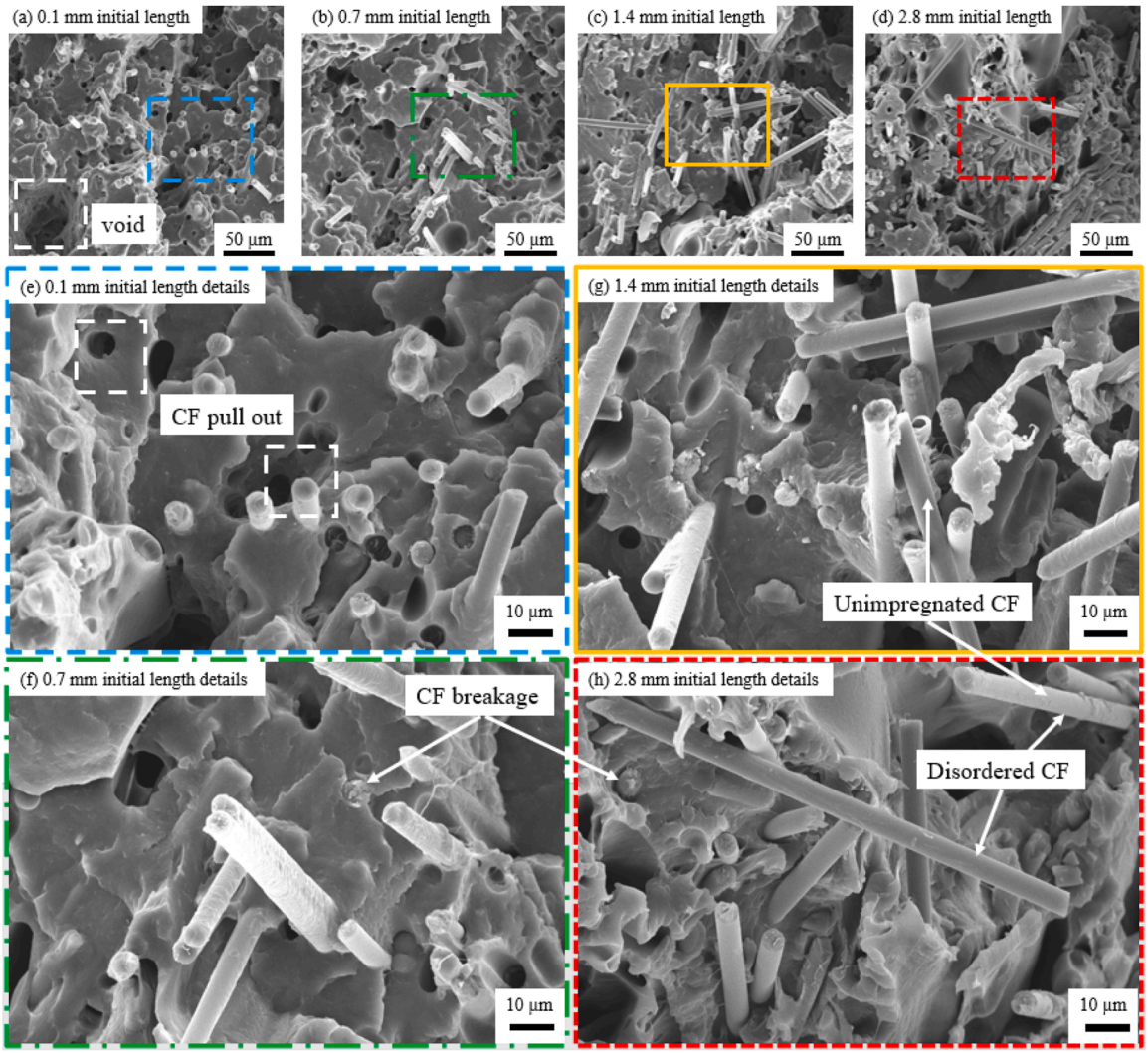

Fig. 8. Fracture surface morphology of FFF printed rCF/PA6 composites.

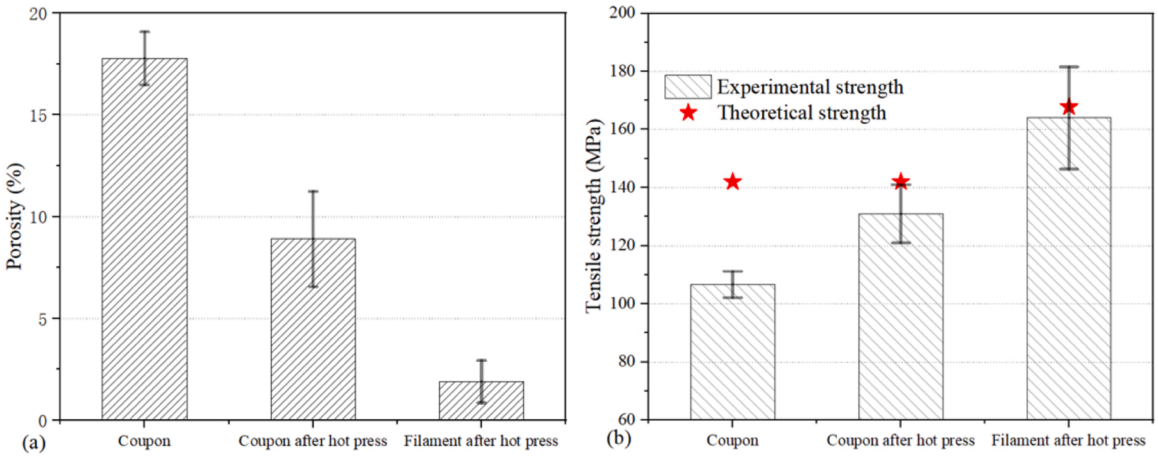

Fig. 9. The porosity (a) and tensile strength (b) of coupons and filaments after hot pressing.

internal pressure within the nozzle. For instance, modifying the internal shape of the nozzle to change flow channel which has been theoretically validated in our previous work through a CFD-FEM model [22]. Alternatively, increasing the internal space or outlet of the nozzle is also an option [32], however it will make fibre disorder. The second stage of fibre breakage is a result of shearing and bending experienced by the fibres as they exit the nozzle and contact with the bed. To address this, increasing the layer height can be beneficial, as demonstrated by Yang et al. [32]. In conclusion, minimizing the resistance to the polymer flow during the printing process is pivotal to enhancing the printing of

discontinuous fibre composites. The generation of voids and the sub-optimal CF/matrix interface are mainly influenced by the increased viscosity of the polymer. This can be improved by adjusting the printing parameters, such as reducing the printing speed and increasing the bed temperature. Additionally, a significant improvement to this issue has been proposed by Zhang et al. through a laser-assisted 3D printing process, which holds considerable promise [50].

Totally, the hot-pressed filaments have a 55.6% improvement in tensile strength compared to the strength of the printed coupons. This enhancement can be attributed to the fact that the fibres in the hot-pressed filaments retain optimal state and the porosity is minimized. Therefore, it is discovered that the tensile strength of the FFF printed 20 wt% rCF/PA6 composite can be potentially leveraged by 55.6% by maintaining the fibre length (*i.e.*, 750 μm fibre length which is above the critical length of 700 μm and better fibre orientation) and removing the air voids.

5. Conclusions

In this study, recycled carbon fibres reinforced PA6 flakes were fabricated into filaments for material extrusion FFF 3D printing. With a fibre fraction of 20 wt%, the composite flakes containing recycled carbon fibres from 100 μm to 2.8 mm were extruded, printed, tested and characterised to investigate how the material microstructures evolve and identify how such changes contribute to the mechanical property loss of the printed composites. Fibre length, fibre orientation, as well as porosity during the screw-based extrusion and FFF printing processes, were quantified and analysed. The research serves a necessary preliminary exploration for achieving additive manufacturing of long fibre reinforced composites. Follow conclusions are drawn.

- The mechanical properties of the FFF printed rCF/PA6 composites are apparently affected by the fibre length, especially the tensile strength and tensile modulus of the printed composites are significantly enhanced with the increase of fibre length.
- There are limitations in the current FFF printing of discontinuous fibre reinforced composites. It led to shortened fibre length, weak fibre/matrix interface and anisotropic fibre orientation. These defects are magnified as the fibre length increases.
- The tensile strength of FFF printed discontinuous CF/PA6 composites with a 20 wt% fibre fraction and an original fibre length in filaments of 750 μm could be improved up to 55.6%, indicating the significance for further developing the additive manufacturing technique.

Further research will be required in future to improve the material extrusion additive manufacturing process to better preserve fibre efficiency and reduce air voids.

CRediT authorship contribution statement

Jiang Wu: Writing – original draft, Methodology, Investigation, Data curation, Conceptualization. **Ka Zhang:** Writing – review & editing, Visualization, Software. **Dongmin Yang:** Writing – review & editing, Supervision, Conceptualization.

Declaration of Competing Interest

The authors have no conflicts of interest related to this publication.

Data Availability

Data will be made available on request.

Acknowledgements

This research did not receive any specific grant from funding agencies in the public, commercial, or not-for-profit sectors.

Appendix A. Fibre orientation and length measurement

As Fig. A1a shows, since it is hard to ensure that the initial build orientation of filaments and coupons is parallel to the image direction, it is necessary to determine the initial direction of coupons and filaments in images. Thus, the average angle (θ) between fibre orientation and image direction was considered to be the initial build orientation (See Fig. A1b).

$$\overline{\theta} = \frac{\Sigma_{i=1}^{n}\theta_i}{n} \tag{A1}$$

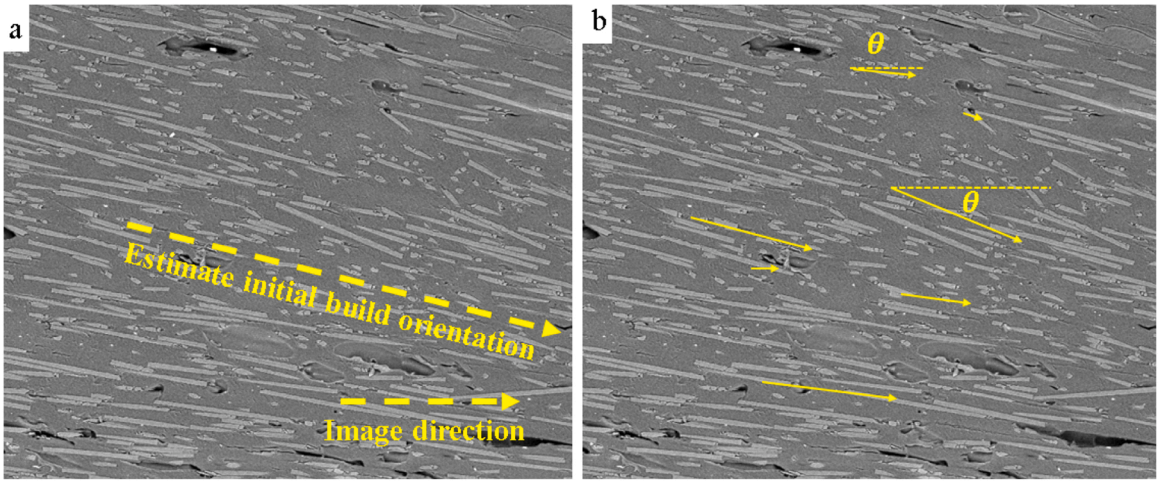

Fig. A1. Definition of initial build orientation for fibre orientation measurement: (a) initial build orientation and image direction are inconsistent, thus (b) θ of each fibre was highlighted to define the initial build orientation.

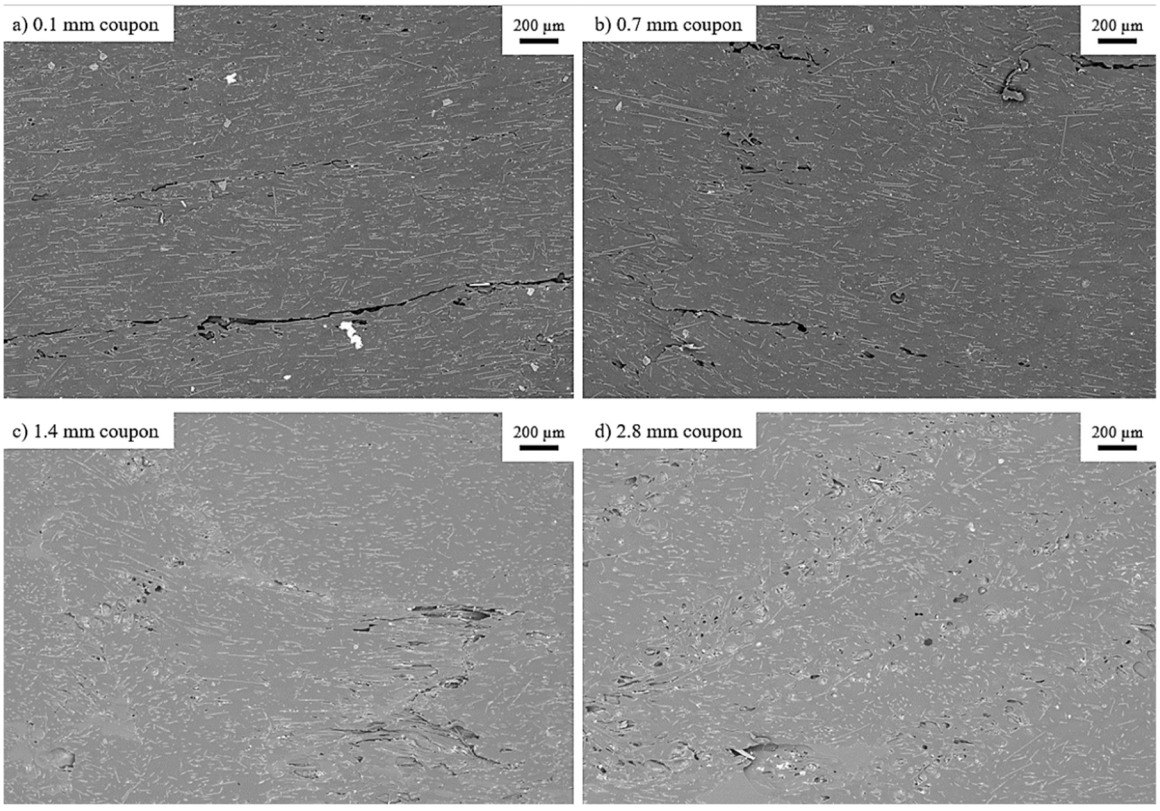

Fig. A2. SEM images of coupons for fibre orientation measurement.

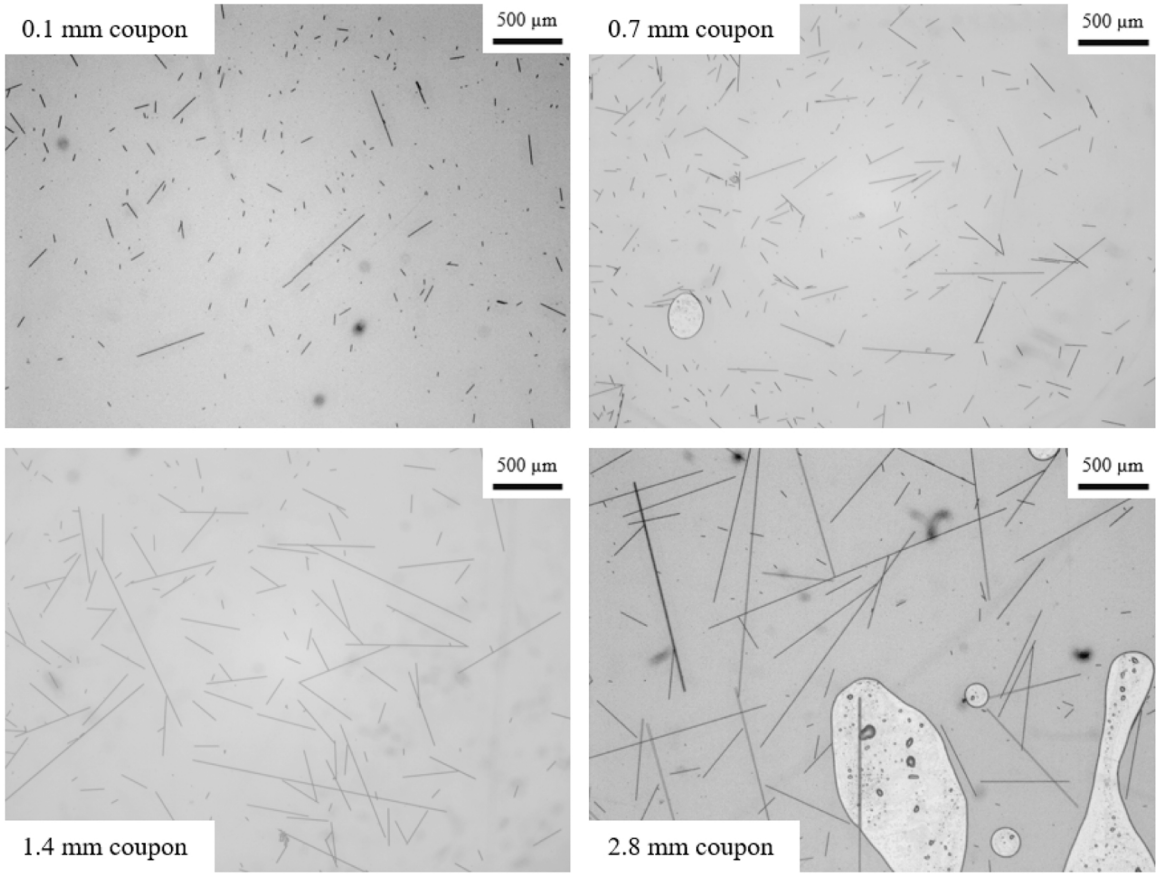

Fig. A3. Microscopic images of coupons for fibre length measurement.

References

[1] The Worldwide Recycled Carbon Fiber Industry is Expected to Reach $222 Million by 2026, ⟨https://www.globenewswire.com/en/news-release/2022/03/30/2412546/28124/en/The-Worldwide-Recycled-Carbon-Fiber-Industry-is-Expected-to-Reach-222-Million-by-2026.html⟩, 2022.

[2] K. Wong, C. Rudd, S. Pickering, X. Liu, Composites recycling solutions for the aviation industry, Sci. China Technol. Sci. 60 (9) (2017) 1291–1300.

[3] P. Ghabezi, T. Flanagan, N. Harrison, Short basalt fibre reinforced recycled polypropylene filaments for 3D printing, Mater. Lett. 326 (2022), 132942.

[4] N. Dixit, P.K. Jain, 3D printed carbon fiber reinforced thermoplastic composites: a review, Mater. Today.: Proc. (2021).

[5] L.G. Blok, M.L. Longana, H. Yu, B.K.S. Woods, An investigation into 3D printing of fibre reinforced thermoplastic composites, Addit. Manuf. 22 (2018) 176–186.

[6] N. Su, R.S. Pierce, C. Rudd, X. Liu, Comprehensive investigation of reclaimed carbon fibre reinforced polyamide (rCF/PA) filaments and FDM printed composites, Compos. Part B: Eng. 233 (2022), 109646.

[7] R.T.L. Ferreira, I.C. Amatte, T.A. Dutra, D. Bürger, Experimental characterization and micrography of 3D printed PLA and PLA reinforced with short carbon fibers, Compos. Part B: Eng. 124 (2017) 88–100.

[8] L.J. Love, V. Kunc, O. Rios, C.E. Duty, A.M. Elliott, B.K. Post, R.J. Smith, C.A. Blue, The importance of carbon fiber to polymer additive manufacturing, J. Mater. Res. 29 (17) (2014) 1893–1898.

[9] H.L. Tekinalp, V. Kunc, G.M. Velez-Garcia, C.E. Duty, L.J. Love, A.K. Naskar, C. A. Blue, S. Ozcan, Highly oriented carbon fiber–polymer composites via additive manufacturing, Compos. Sci. Technol. 105 (2014) 144–150.

[10] W.G. Emmett Hull, Meng Zhang, Xiaoxu Song, Z.J. Pei, Weilong Cong, Effects of Process Variables on Extrusion of Carbon Fiber Reinforced ABS Filament for Additive Manufacturing ASME 2015 International Manufacturing Science and Engineering Conference, ASME, Charlotte, North Carolina, USA, 2015.

[11] J. Li, Y. Durandet, X. Huang, G. Sun, D. Ruan, Additively manufactured fiber-reinforced composites: a review of mechanical behavior and opportunities, J. Mater. Sci. Technol. 119 (2022) 219–244.

[12] C. Hu, Q.-H. Qin, Advances in fused deposition modeling of discontinuous fiber/polymer composites, Curr. Opin. Solid State Mater. Sci. 24 (5) (2020), 100867.

[13] S.Y. Fu, B. Lauke, E. Mäder, C.Y. Yue, X. Hu, Tensile properties of short-glass-fiber- and short-carbon-fiber-reinforced polypropylene composites, Compos. Part A: Appl. Sci. Manuf. 31 (10) (2000) 1117–1125.

[14] P.K. Mallick, 5 - Thermoplastics and thermoplastic–matrix composites for lightweight automotive structures, in: P.K. Mallick (Ed.), Materials, Design and Manufacturing for Lightweight Vehicles, Woodhead Publishing, 2010, pp. 174–207.

[15] L.G. Blok, M.L. Longana, B.K.S. Woods, Fabrication and characterisation of aligned discontinuous carbon fibre reinforced thermoplastics as feedstock material for fused filament fabrication, Materials 13 (20) (2020) 4671.

[16] A. Bernasconi, F. Cosmi, Analysis of the dependence of the tensile behaviour of a short fibre reinforced polyamide upon fibre volume fraction, length and orientation, Procedia Eng. 10 (2011) 2129–2134.

[17] A. Dey, I.N. Roan Eagle, N. Yodo, A review on filament materials for fused filament fabrication, J. Manuf. Mater. Process. (2021).

[18] Y. Lyu, J. Wu, H. Zhang, C.M.Ó. Brádaigh, D. Yang, Effects of thermal process conditions on crystallinity and mechanical properties in material extrusion additive manufacturing of discontinuous carbon fibre reinforced polyphenylene sulphide composites, J. Compos. Mater. 57 (24) (2023) 3775–3787.

[19] F. Ning, W. Cong, Y. Hu, H. Wang, Additive manufacturing of carbon fiber-reinforced plastic composites using fused deposition modeling: effects of process parameters on tensile properties, J. Compos. Mater. 51 (4) (2016) 451–462.

[20] N. Krajangsawasdi, L.G. Blok, I. Hamerton, M.L. Longana, B.K.S. Woods, D. S. Ivanov, Fused deposition modelling of fibre reinforced polymer composites: a parametric review, J. Compos. Sci. (2021).

[21] F. Ning, W. Cong, J. Qiu, J. Wei, S. Wang, Additive manufacturing of carbon fiber reinforced thermoplastic composites using fused deposition modeling, Compos. Part B: Eng. 80 (2015) 369–378.

[22] A. Kelly, W.R. Tyson, Tensile properties of fibre-reinforced metals: copper/tungsten and copper/molybdenum, J. Mech. Phys. Solids 13 (6) (1965) 329–350.

[23] F. Touchard, L. Chocinski-Arnault, T. Fournier, C. Magro, A. Lafitte, A. Caradec, Interfacial adhesion quality in 3D printed continuous CF/PA6 composites at filament/matrix and interlaminar scales, Compos. Part B: Eng. 218 (2021), 108891.

[24] H. Zhang, L. Zhang, H. Zhang, J. Wu, X. An, D. Yang, Fibre bridging and nozzle clogging in 3D printing of discontinuous carbon fibre-reinforced polymer composites: coupled CFD-DEM modelling, Int. J. Adv. Manuf. Technol. 117 (11) (2021) 3549–3562.

[25] N. Krajangsawasdi, M.L. Longana, I. Hamerton, B.K.S. Woods, D.S. Ivanov, Batch production and fused filament fabrication of highly aligned discontinuous fibre thermoplastic filaments, Addit. Manuf. 48 (2021), 102359.

[26] X. Yan, Y. Yang, H. Hamada, Tensile properties of glass fiber reinforced polypropylene composite and its carbon fiber hybrid composite fabricated by direct fiber feeding injection molding process, Polym. Compos. 39 (10) (2018) 3564–3574.

[27] D. Purslow, The shear of unidirectional carbon fibre reinforced plastics and their experimental determination. MOD CP No. 1381, Ministry of Defence, London, 1976, p. 1976.

[28] C. Hu, W.N.G.J. Hau, W. Chen, Q.-H. Qin, The fabrication of long carbon fiber reinforced polylactic acid composites via fused deposition modelling: experimental analysis and machine learning, J. Compos. Mater. (2020), 0021998320972172.

[29] E. Verdejo de Toro, J. Coello Sobrino, A. Martínez Martínez, V. Miguel Eguía, J. Ayllón Pérez, Investigation of a short carbon fibre-reinforced polyamide and comparison of two manufacturing processes: fused deposition modelling (FDM) and polymer injection moulding (PIM), Materials 13 (3) (2020) 672.

[30] A.L. Woern, J.R. McCaslin, A.M. Pringle, J.M. Pearce, RepRapable Recyclebot: open source 3-D printable extruder for converting plastic to 3-D printing filament, HardwareX 4 (2018), e00026.

[31] A. Matschinski, P. Ziegler, T. Abstreiter, T. Wolf, K. Drechsler, Fiber formation of printed carbon fiber/poly (Ether Ether Ketone) with different nozzle shapes, Polym. Int. 70 (8) (2021) 1109–1117.

[32] N. Zhang, J. Sanjayan, Extrusion nozzle design and print parameter selections for 3D concrete printing, Cem. Concr. Compos. 137 (2023), 104939.

[33] D. Yang, H. Zhang, J. Wu, E.D. McCarthy, Fibre flow and void formation in 3D printing of short-fibre reinforced thermoplastic composites: an experimental benchmark exercise, Addit. Manuf. 37 (2021), 101686.

[34] Z. Yang, Z. Yang, H. Chen, W. Yan, 3D printing of short fiber reinforced composites via material extrusion: fiber breakage, Addit. Manuf. 58 (2022), 103067.

[35] C. Pascual-González, P. San Martín, I. Lizarralde, A. Fernández, A. León, C.S. Lopes, J.P. Fernández-Blázquez, Post-processing effects on microstructure, interlaminar and thermal properties of 3D printed continuous carbon fibre composites, Compos. Part B: Eng. 210 (2021), 108652.

[36] ASTM 3039-D3039M-14 StandardTest Method for Tensile Properties of Polymer Matrix Composite Materials1, ASTM, international, West Chonshohcken, 2014.

[37] ASTM D638–14 Standard Test Method for Tensile Properties of Plastics, ASTM, Internaltional, West Conshohocken, 2014.

[38] D. Jiang, D.E. Smith, Anisotropic mechanical properties of oriented carbon fiber filled polymer composites produced with fused filament fabrication, Addit. Manuf. 18 (2017) 84–94.

[39] X. Li, J. He, Z. Hu, X. Ye, S. Wang, Y. Zhao, B. Wang, Y. Ou, J. Zhang, High strength carbon-fiber reinforced polyamide 6 composites additively manufactured by screw-based extrusion, Compos. Sci. Technol. 229 (2022), 109707.

[40] L. Sang, S. Han, Z. Li, X. Yang, W. Hou, Development of short basalt fiber reinforced polylactide composites and their feasible evaluation for 3D printing applications, Compos. Part B: Eng. 164 (2019) 629–639.

[41] T. Shafighfard, T.A. Cender, E. Demir, Additive manufacturing of compliance optimized variable stiffness composites through short fiber alignment along curvilinear paths, Addit. Manuf. (2020), 101728.

[42] N.G. Karsli, A. Aytac, V. Deniz, Effects of initial fiber length and fiber length distribution on the properties of carbon-fiber-reinforced-polypropylene composites, J. Reinf. Plast. Compos. 31 (15) (2012) 1053–1060.

[43] J.J. Fallon, S.H. McKnight, M.J. Bortner, Highly loaded fiber filled polymers for material extrusion: a review of current understanding, Addit. Manuf. 30 (2019), 100810.

[44] O. Sam-Daliri, P. Ghabezi, J. Steinbach, T. Flanagan, W. Finnegan, S. Mitchell, N. Harrison, Experimental study on mechanical properties of material extrusion additive manufactured parts from recycled glass fibre-reinforced polypropylene composite, Compos. Sci. Technol. 241 (2023), 110125.

[45] W. Liu, H. Huang, L. Zhu, Z. Liu, Integrating carbon fiber reclamation and additive manufacturing for recycling CFRP waste, Compos. Part B: Eng. 215 (2021), 108808.

[46] F. Rezaei, R. Yunus, N.A. Ibrahim, Effect of fiber length on thermomechanical properties of short carbon fiber reinforced polypropylene composites, Mater. Des. 30 (2) (2009) 260–263.

[47] H. Huang, W. Liu, Z. Liu, An additive manufacturing-based approach for carbon fiber reinforced polymer recycling, CIRP Ann. 69 (1) (2020) 33–36.

[48] M. Araya-Calvo, I. López-Gómez, N. Chamberlain-Simon, J.L. León-Salazar, T. Guillén-Girón, J.S. Corrales-Cordero, O. Sánchez-Brenes, Evaluation of compressive and flexural properties of continuous fiber fabrication additive manufacturing technology, Addit. Manuf. 22 (2018) 157–164.

[49] K. Wang, S. Pei, Y. Li, J. Li, D. Zeng, X. Su, X. Xiao, N. Chen, In-situ 3D fracture propagation of short carbon fiber reinforced polymer composites, Compos. Sci. Technol. 182 (2019), 107788.

[50] J. Zhang, W. Yang, Y. Li, Process-dependent multiscale modeling for 3D printing of continuous fiber-reinforced composites, Addit. Manuf. 73 (2023), 103680.